AFRL-OSR-VA-TR-2014-0008

DIELECTRIC BARRIER DISCHARGE PLASMA ACTUATORS WITH NOVEL GEOMETRIES FOR FLOW MODIFICATION EXPERIMENTAL MEASUREMENTS AND VALIDATION WITH A 2-D FLUID MODEL

NOAH HERSHKOWITZ

UNIVERSITY OF WISCONSIN SYSTEM

12/30/2013
Final Report

AIR FORCE RESEARCH LABORATORY
AF OFFICE OF SCIENTIFIC RESEARCH (AFOSR)/RSE
ARLINGTON, VIRGINIA 22203
AIR FORCE MATERIEL COMMAND

REPORT DOCUMENTATION PAGE

Form Approved
OMB No. 0704-0188

1. REPORT DATE *(DD-MM-YYYY)*	2. REPORT TYPE	3. DATES COVERED *(From - To)*
12/27/2013	Final	09/30/2010 - 09/29/2013

4. TITLE AND SUBTITLE
Dielectric barrier discharge plasma actuators with novel geometries for flow modification: Experimental measurements and validation with a 2-D fluid model

5a. CONTRACT NUMBER
FA9550-10-1-0565

5b. GRANT NUMBER
AFOSR-BAA-2009-1

5c. PROGRAM ELEMENT NUMBER

6. AUTHOR(S)
Hershkowitz, Noah Dr.
Bonazza, Riccardo Dr.

5d. PROJECT NUMBER
PRJ41UJ

5e. TASK NUMBER

5f. WORK UNIT NUMBER

7. PERFORMING ORGANIZATION NAME(S) AND ADDRESS(ES)
UNIVERSITY OF WISCONSIN SYSTEM
RESEARCH & SPONSORED PROGRAMS
21 N PARK ST STE 6401
MADISON WI 53715-1218

8. PERFORMING ORGANIZATION REPORT NUMBER
MSN127770

9. SPONSORING/MONITORING AGENCY NAME(S) AND ADDRESS(ES)
USAF, AFRL DUNS 143574726
AF OFFICE OF SCIENTIFIC RESEARCH
875 NORTH RANDOLPH STREET, RM 3112
ARLINGTON VA 22203

10. SPONSOR/MONITOR'S ACRONYM(S)
AFOSR

11. SPONSOR/MONITOR'S REPORT NUMBER(S)
SF-298

12. DISTRIBUTION/AVAILABILITY STATEMENT

Approved for public release; distribution is unlimited

13. SUPPLEMENTARY NOTES
None

14. ABSTRACT
See attached

15. SUBJECT TERMS
Dielectric barrier discharge (DBD)

16. SECURITY CLASSIFICATION OF:			17. LIMITATION OF ABSTRACT	18. NUMBER OF PAGES	19a. NAME OF RESPONSIBLE PERSON
a. REPORT	b. ABSTRACT	c. THIS PAGE			Noah Hershkowitz
					19b. TELEPHONE NUMBER *(Include area code)*
U	U	U	UU	16	608-831-5862

SF-298 Abstract / Contract No. FA9550-10-1-0565

Optical characteristics of surface dielectric barrier discharge (DBD) plasma actuators with wire/planar electrodes were studied using an intensified charge-coupled device camera and a monochromator in atmospheric pressure air. Spatial and temporal images were recorded both parallel and perpendicular to actuator surfaces on nanosecond time scales. By tilting the actuator surface, arc-shaped discharges jumping from above the powered wire across the dielectric above the grounded planar electrode were observed for the first time. Time resolved velocity measurements of the air flow fields induced by planar DBD actuators were also made by phase contrast imaging of buoyant plumes passing through the discharge. Studies of the use of DBDs to prevent flow separation from the suction side of an airfoil in air demonstrated that separation-control depends on the size of the exposed electrodes and the amplitude of the applied voltage. Suppression of separation was seen in both flow visualization images and in measurements of the lift produced by the airfoil. Coaxial radio frequency atmospheric pressure air plus helium DBDs with one electrode covered with glass were also investigated. The coaxial design allowed operation with very low power density plasmas and a much larger plasma size than the parallel plate designs.

Dielectric barrier discharge plasma actuators with novel geometries for flow modification: Experimental measurements and validation with a 2-D fluid model

FA9559-10-1-0565, AFOSR, Final Report 12/28/2013

Noah Hershkowitz, Riccardo Bonazza
University of Wisconsin-Madison

Abstract

Optical characteristics of surface dielectric barrier discharge (DBD) plasma actuators with wire/planar electrodes were studied using an intensified charge-coupled device camera and a monochromator in atmospheric pressure air. Spatial and temporal images were recorded both parallel and perpendicular to actuator surfaces on nanosecond time scales. By tilting the actuator surface, arc-shaped discharges jumping from above the powered wire across the dielectric above the grounded planar electrode were observed for the first time. Time resolved velocity measurements of the air flow fields induced by planar DBD actuators were also made by phase contrast imaging of buoyant plumes passing through the discharge. Studies of the use of DBDs to prevent flow separation from the suction side of an airfoil in air demonstrated that separation-control depends on the size of the exposed electrodes and the amplitude of the applied voltage. Suppression of separation was seen in both flow visualization images and in measurements of the lift produced by the airfoil. Coaxial radio frequency atmospheric pressure air plus helium DBDs with one electrode covered with glass were also investigated. The coaxial design allowed operation with very low power density plasmas and a much larger plasma size than the parallel plate designs.

Introduction

A dielectric barrier discharge (DBD) is a system in which plasma forms between two electrodes, which have at least one dielectric layer between them, with an alternating voltage applied between the electrodes. In the absence of a dielectric layer, the plasma would quickly make a transition to a thermal arc discharge. In a DBD, the plasma deposits charge on the dielectric layer, shielding out the electric field in the gas region, preventing this transition. The plasma in a DBD forms and extinguishes at least once, and often many times, during each half cycle of the oscillating applied voltage.

Several DBD designs are shown in Figure 1. Parallel-plate designs, shown in Figure 1a, are often employed in materials processing applications. The concentric cylinder design of Figure 1b was designed by Siemens in 1857 to generate ozone, and is still widely used for that purpose today (Kogelschatz, 2004). Plasma actuators that provide airflow modifications over surfaces are shown in Figures 1c and 1d. Note that Figure 1d has the advantage that the actuator surface is a smooth dielectric.

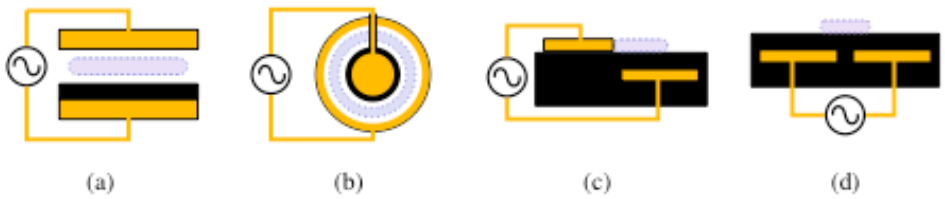

Figure 1: Common DBD configurations, showing electrodes, dielectric materials (in black), and the approximate plasma regions (inside dashed outlines). The drawings show (a) a single-barrier parallel-plate discharge, (b) a single-barrier concentric discharge, (c) a single-barrier surface discharge and (d) a double-barrier surface discharge, also called a coplanar discharge.

Work over the grant period has employed DBDs similar to Figures 1b, 1c and 1d. Triangular as opposed to sinusoidal voltage waveforms were employed in many of our investigations.

Many groups have demonstrated that DBDs generating plasma on a flat surface, using the asymmetric electrode configuration shown schematically in Figure 1c can induce a flow of neutral gas when operated in ambient air. This induced flow is shown schematically in Figure 2a. Experiments reported in the previous grant period studied actuators with wire-strip geometries, shown in Figure 2b, found the induced force increased almost exponentially as the wire diameter decreased.

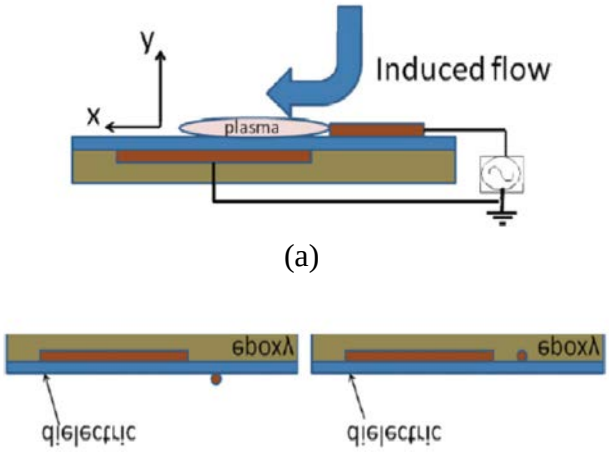

Figure 2: (a) Conceptual diagram of a DBD plasma actuator showing electrodes (brown), dielectric (blue), and approximate direction of induced airflow. (b) Detail of single and double barrier actuators with wire/strip electrodes.

DBDs have been shown to operate in two distinct modes, which can exist simultaneously: diffuse and filamentary. A comparison of the microdischarges near the bottom of the negative going half cycle (−11,400 V) and near the peak of the positive going half cycle (+11,400 V) is given in Figures 3a and b, respectively. The photos for the negative and

positive going voltages show similar overall structures in opposite directions, but the negative going one has shorter, branch-like filaments and longer diffuse, jet-like structures.

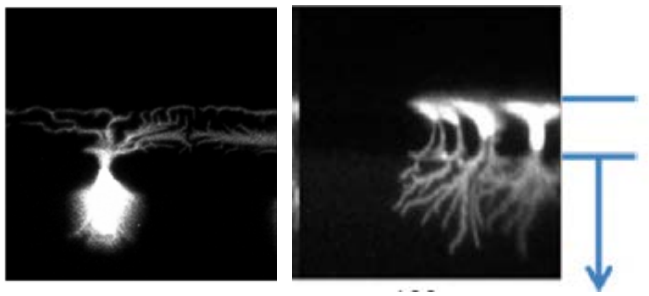

(a) (b)

Figure 3: ICCD images with 100 ns gate width taken (*a*) near the bottom of the negative going half cycle (*b*) near the peak of the positive going half. The blue lines on the right indicate the position of the wire and the boundary of the strip.

Plasma Actuator Modeling

Early in the current grant period, details were published of the two-dimensional fluid simulation of the plasma dynamics in surface dielectric barrier discharges operating in air [1]. This material was presented in the final report of the previous grant period. Previous simulations of such discharges modeled the electrodes as thin strips. The new code also considered plasma actuators with various sizes of cylindrical electrodes. In single-barrier actuators, the size of the exposed electrode qualitatively affects the discharge dynamics, particularly with a negative-going applied voltage. For both geometries, the simulations predicted the formation of plasma structures similar to those imaged in previous experiments. Experimentally observed increases in forces for actuators with smaller high-voltage electrodes were reproduced for the single-barrier geometry. That experimental result was a major experimental finding of the previous grant period. Results are shown in Figure 4.

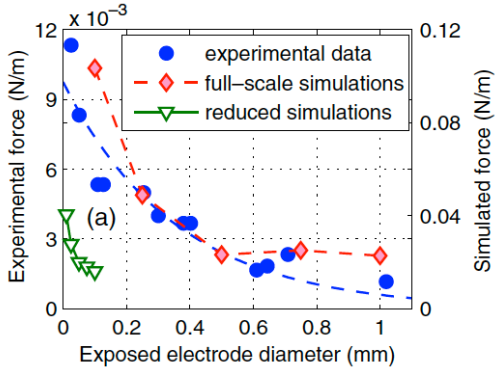

Figure 4: Simulated and measured time-averaged forces for single-barrier actuators as a function of wire thickness.

Phase Contrast Imaging of Induced Airflow Topologies

Spatial and temporal evolution of both air flow and plasma fields in parallel and asymmetric atmospheric pressure DBDs were analyzed with the help of phase contrast imaging and a gated ICCD [2], [3]. Buoyancy plumes rising from resistively heated tungsten wires along with the phase contrast technique were used to study the induced flow topology. The experiment was carried out using several electrode diameters/widths, applied high voltages and frequencies. Correlation between the electrode dimension, size of induced swirls above the exposed electrode and induced body force was identified. Time-resolved phase contrast imaging of buoyant plumes passing through the discharge was used to measure the instantaneous velocity of various flow fields.

Optical measurements of DBD actuators

Previous optical measurements of DBD plasma actuators have been made in the x-z plane of the actuator. These measurements showed a combination of filamentary and diffuse and structures. Because of this, modeling of actuator operation has also concentrated on streamer propagation in the actuator plane. There has been an absence of data in the y-z plane perpendicular to the actuator plane and an absence of modeling of the electrical discharge characteristics in the y-z plane. During the current grant period, experimental studies of filamentary structures in the y-z plane were carried out [4].

Experimental set-up for optical measurements

The voltage waveform was a triangular 1 kHz signal produced by a signal generator. A Trek 20/20B high voltage amplifier was used. The output of the amplifier was connected to the narrow electrode and the wide electrode was grounded. In order to avoid plasma formation under the dielectric layer, this space was filled with Stycast 2651-40 epoxy. The x–y plane, i.e. the side view of the actuator and the x–z plane, the top view of the actuator are shown schematically in Figures 5a and b respectively.

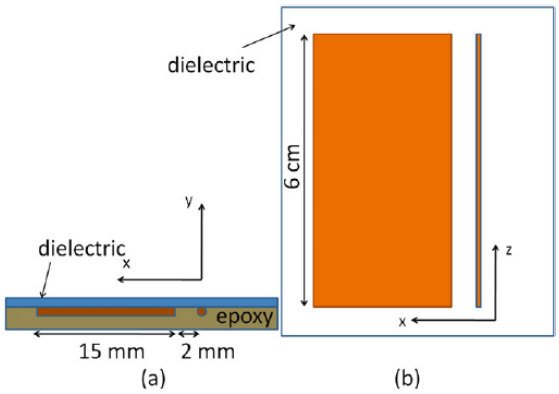

Figure 5: Double barrier actuator schematic showing (a) side view and (b) top view.

The ICCD camera positions are shown in Figure 6. The ICCD camera was placed either parallel (Figure 6a) or perpendicular (Figure 6b) to the plane of the aerodynamic actuator. Measurements of microdischarge formation and propagation were performed using a

Princeton Instrument Acton Series Monochromator (PI-MAX) ICCD camera. Optical emission discharge spectra were taken with a .500m focal length.

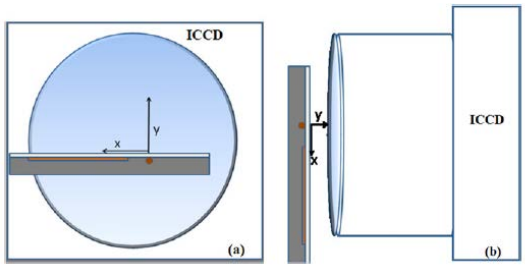

Figure 6: The ICCD camera positions with (a) parallel and (b) perpendicular to the actuator surface.

When the ICCD camera was placed perpendicular to the actuator surface, separate microdischarges were apparent. The time evolution of the discharge near the peak of the positive half cycle is given in Figure 7.

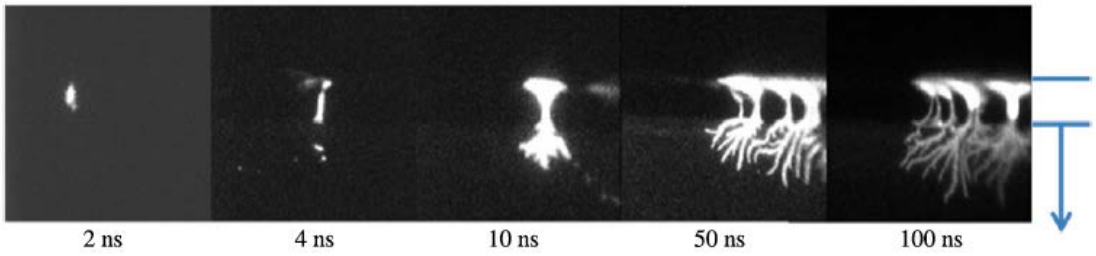

Figure 7: Images taken by the ICCD camera perpendicular to the actuator surface labeled by the gate width.

Double barrier microdischarges exhibited diffuse and filamentary modes simultaneously. The camera was triggered to open at 0.24 ms corresponding to 11,520 V and was not triggered by individual discharges. Numerous shots were taken to catch the random microdischarges. An upwardly moving diffuse discharge 2mm in length that initiated above the narrow electrode was apparent for the 2 ns gate. The 4 ns photo shows a diffuse discharge that expanded to 4 mm in length (2 mm beyond the edge of the other conductor) as well as the beginnings of a downward moving filamentary discharge. The simultaneous filamentary and diffuse nature of the discharges was already apparent for the 10 ns gate width. The 50 ns data showed the presence of multiple discharges across the aerodynamic actuator. The photos only view 2 cm of the 6 cm wide actuators so it is likely that multiple discharges occurred during the shorter duration gate widths but were outside the field of view. The line to the right of the discharge in the 10 ns window may be evidence of an additional discharge. The discharge width in Figure 7 versus time can be seen in Figure 8.

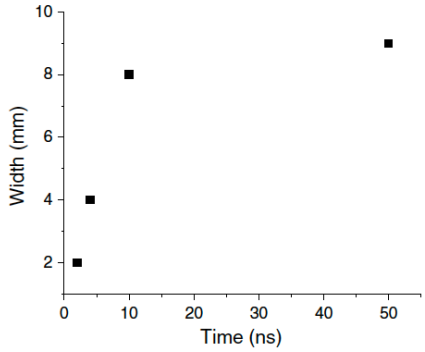

Figure 8: The discharge length versus gate width for perpendicular view.

The discharge width was 4 mm for 4 ns exposure time and this corresponds to at least a 10^6 ms^{-1} discharge velocity because the entire discharge may not have been captured.

When the ICCD camera is placed perpendicular to the actuator surface, separate microdischarges can be discerned, but when it is placed parallel to the surface, it is very difficult to separately distinguish multiple simultaneous discharges because they overlap in the photos. Multiple simultaneous overlapping microdischarge images were captured at different gate widths when the camera was parallel to the actuator surface, as seen in Figure 9.

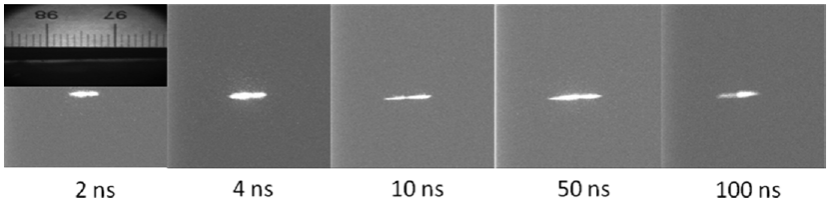

Figure 9: Images of ICCD camera parallel to the actuator surface.

Figure 10 shows that there was an increase over time in the average microdischarge length, and that the expansion was not uniform. The discharge width was 4 mm for a 2 ns exposure time, which corresponds to a velocity of at least 2×10^6 ms^{-1}, in agreement with the data taken in the perpendicular direction.

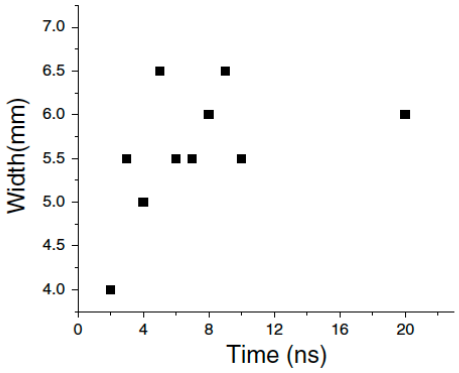

Figure 10: The discharge width versus gate width for parallel view.

By tilting the actuator at a small angle it was possible to eliminate most of the bright discharge region from the ICCD camera's view. Surprisingly, an arc-shaped discharge above the dielectric was seen for the first time, as seen in Figure 11.

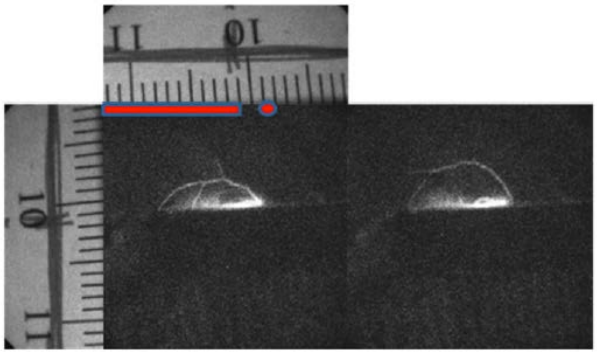

Figure 11: Two ICCD pictures with actuator tilted a small angle from the parallel position. The exposure time was 1 ms. 1 mm divisions indicate the spatial dimensions.

The semicircular structure had a 9 mm width and a 2–4 mm height for a 1 ms gate width during the positive going cycle. The evolution of the arc-like structure can be inferred from Figure 12, which shows arc-shaped structures observed for different gate widths.

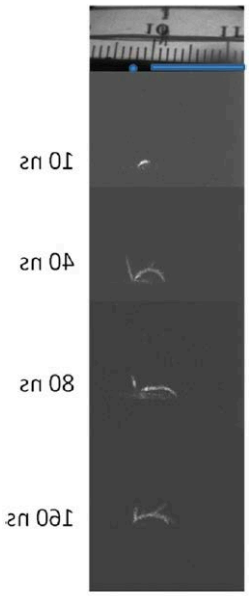

Figure 12: Double barrier actuator arc-shaped structure images at different gate widths.

Note that each photo records a different event. It was apparent that the arc-shaped structure originated near the narrow electrode and ended well beyond the gap. Initially they appeared as a semicircle above the discharge and eventually they branched. Such arcs were only observed during the positive going cycle and coexisted with discharges parallel and close to the surface, as seen in Figure 11. The width of the arc-shaped

structure in the x direction is given as a function of gate width in Figure 13. The maximum speed was at least 10^5 ms^{-1}.

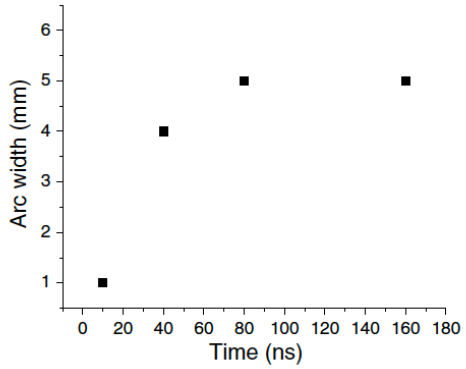

Figure 13: Arc-shaped structure width increases with camera gate width.

Arc-shaped structures were also observed for a single barrier actuator during the negative going half cycle, as shown in Figure 14, but were not seen during the positive going half cycle.

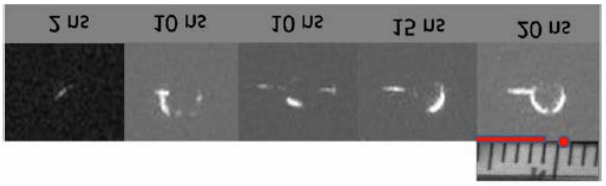

Figure 14: Single barrier actuator arc-shaped structure images at different gate widths.

Unlike the double barrier actuator, the separation of the wire electrode (0.03 mm diameter) and planar electrode was 1 mm. At 2 ns, an arc-shaped structure was seen emerging from above the powered wire electrode. By 10 ns, a fully formed arc-shape was apparent, but the right half appeared to be an afterglow image of the discharge immediately before the gate was opened. By 20 ns, the full arc-shaped structure followed by a flat portion was apparent. The arc widths for single and double barrier actuators were both approximately twice the electrode separation distance. The structures above single barrier actuators appeared to form on a shorter time scale. These structures only appeared during the negative going part of the half cycle, while the structures above the double barrier actuators were only observed during the positive going half cycle.

These results provide clear evidence that substantial physics was taking place in the plane perpendicular to the surface of the actuator. Thus it is important to extend modeling of DBD actuator performance to three dimensions.

DBD elimination of flow separation over wing surfaces

Work in recent years has shown that airflow control by plasma actuators on the leading edges and surfaces of airfoils can delay or eliminate flow separation. Flow separation increases the drag and reduces the lift of airfoils. As shown in Figures 1c and 1d,

actuators can be constructed with one covered electrode or with both electrodes covered with dielectrics, i.e., as single or double barrier DBD actuators.

Our previous studies of DBD actuators showed that the use of a cylindrical wire exposed electrode was effective in generating airflow momentum in the still air case, suggesting promise as a tool for flow control. The next step, which was taken during the current grant period, was to test this particular DBD configuration on an actual wing at an angle of attack in a free stream [5], [6].

Wing modification and experimental setup for wing measurements

An existing wing, with an NACA2412 cross section, chord length c=30 cm and span b=90 cm, was equipped with two electrodes to operate as a DBD. An exposed electrode (a tungsten wire with diameter, ϕ, ranging from 13 to 100 mm) was placed on the wing's suction side, 20 mm inward of the leading edge. The buried electrode consisted of a rectangular strip of copper tape (15×800×0.1 mm) attached to the wing's suction side, 2 mm downstream of the exposed electrode, covered by a layer of polyester, 0.25 mm thick. The electrodes were connected to a Trek 20/20C power supply. The wing was mounted to a six-component sting balance with adjustable pitch attitude. The wing was tested in a wind tunnel whose test section measures 1.8 m in length, 1.2 m in depth, 0.9 m in height. The maximum speed achievable in the test section was 90 m/s although, with the wing used in these experiments, the sting balance load limit was exceeded at an airspeed of approximately 45 m/s. In the experiments, the freestream velocity was kept at 6 m/s, corresponding to a Reynolds number of approximately 1,000. This particular speed was selected as it is the speed generated in still air by the same kind of plasma discharge used in the wind tunnel experiments. The wing was positioned at angles of attack, α, of 12^o, 13^o, 15^o and 17^o; and peak voltages of 7, 8, and 9 kV were applied across the electrodes. Thus a three-dimensional parameter space was explored (exposed electrode diameter; angle of attack; applied voltage).

Flow visualization

The flow pattern, and in particular the occurrence of flow separation, was studied using a simple flow visualization system based on a theater-type smoke generator and front lighting provided by a white floodlight. Images were recorded using a 35 mm digital SLR camera. Representative images are shown in Figure 15.

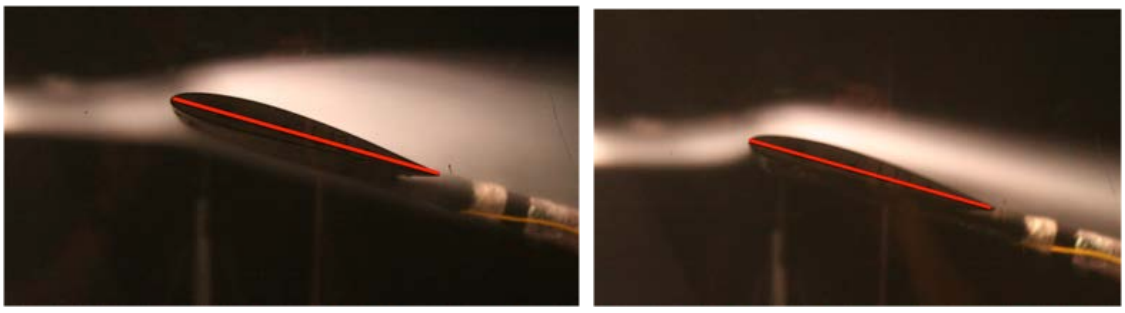

(a) (b)

Figure 15: Flow visualization for the case of 50 mm exposed electrode; 12^o angle of attack; 7 kV peak voltage. (a): Flow separation occurs when the DBD is off. (b): The flow reattaches when the DBD is turned on.

The overall results are summarized in Table 1. The general trend was that reattachment was achieved with lower peak voltages as the diameter of the exposed electrode decreased.

ϕ (μm) / α	13	25	50	100
12^o	7 kV	7 kV	7 kV	No reattachment
13^o	7 kV	7 kV	8 kV	No reattachment
15^o	8 kV	8 kV	9 kV	No reattachment
17^o	7 kV	9 kV	9 kV	No reattachment

Table 1: Minimum peak voltages necessary to observe reattachment.

Force measurements

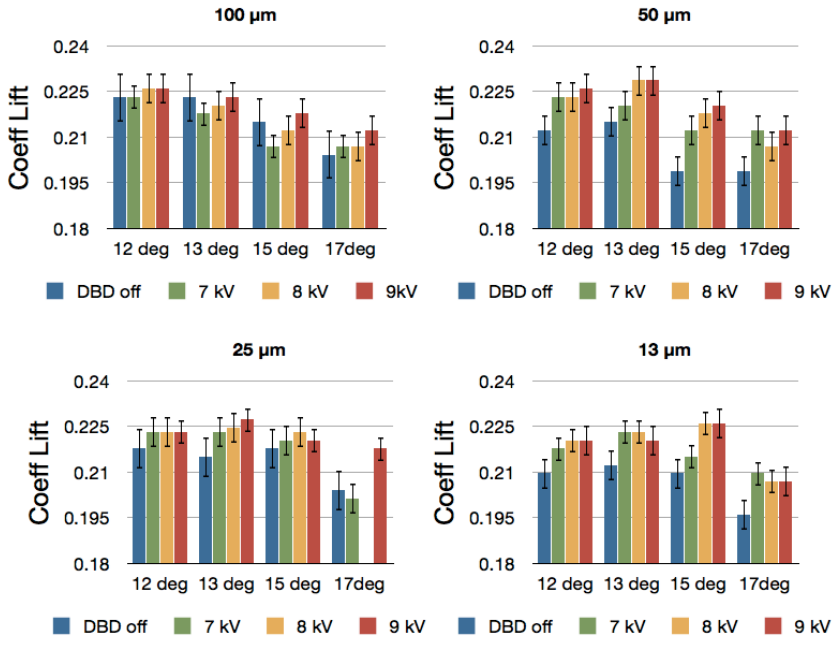

Figure 16: Measurements of lift for four different electrode diameters.

One effect of flow separation was a decrease in lift compared to the case of attached flow. Thus, at any angle of attack, measuring the lift with the DBD off and on provided a

separate means to determine the extent to which the plasma discharge caused the flow to reattach. The results of the force measurements are described in Figure 16. The lift values reported here were the averages of 200 recordings at each angle of attack/electrode diameter/voltage combination. The changes in lift between the DBD-OFF and the DBD-ON cases showed the same trend as the flow visualization results: flow reattachment generated an increase in lift; the smaller the exposed electrode diameter, the lower the voltage required to achieve the same increase in lift.

Coaxial rf DBD with He operating at atmospheric pressure air

During the grant period, coaxial rf DBD air-helium plasma was studied in order to better understand the characteristics of large volume discharges [7]. The coaxial design allowed operation with very low power density plasmas (0.18 W/cm^3) and a much larger plasma size (13 mm) than the parallel plate designs. Two operating modes were identified. In the α mode, trapped electrons provided volumetric ionization throughout the bulk plasma. In the γ mode, energetic electrons heated in the sheath provided local ionization at a much higher rate. Optical studies carried out with parallel plate electrodes, with separations the order of 2 mm, found that emission intensities were highest in the bulk plasma for the α mode consistent with electron trapping and highest near the electrodes in the γ mode consistent with the sheath electron heating. These studies found that the discharge intensities were periodic at the rf driving frequency with the brightest images at T/4 and 3T/4, where T is the rf period, taken at the discharge current peaks and also showed that the bright emitting layers got thinner and closer to the electrodes when the frequency increased.

In a recent publication, Shang et al. modeled atmospheric pressure discharges in helium for a coaxial electrode configuration with both electrodes covered with dielectric barriers. In addition to the α and γ modes corresponding to low and high rf current respectively, they found the discharge was asymmetric with a higher ionization near the central electrode. Addition of argon or helium flow was very important for uniform and stable glow-like plasma generation because of the Penning ionization by metastable argon or helium atoms.

During the grant period, optical images resolved in time and space and optical emission spectra of atmospheric pressure dielectric barrier coaxial capacitively coupled rf discharges were investigated with helium flow in air and compared with previously modeled results.

A schematic diagram of the experimental setup is given in Figure 17. A grounded 2 mm diameter stainless steel electrode was placed on the axis of a glass cylinder, 3.0 cm in diameter and 22.5 cm in length. Rf power at 13.56 MHz was applied to the outer cylindrical rf copper electrode (11.4 cm in length). Helium was introduced with controlled flow rate through the tube on the top while the ends of the cylinder were left open to air. This configuration differed from the one considered by Shang et al. in that the central electrode was not covered by a dielectric.

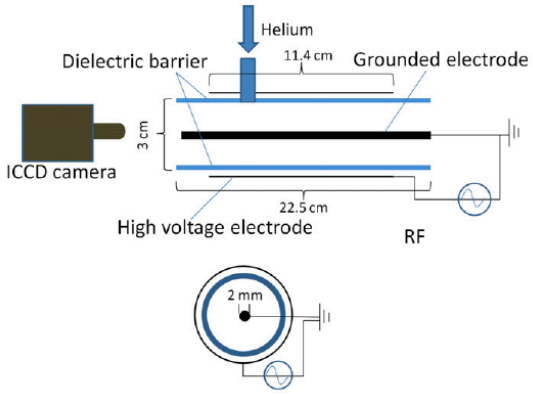

Figure 17: Schematic of cylindrical discharge tube.

The evolution of the discharge light emission in one rf cycle was recorded using a Princeton PI-MAX Intensified Charge Coupled Device (ICCD) camera. Optical emission was collected with a Princeton Instrument Ac-ton SP 2500i (0.500 meter focal length) monochromator. A double probe consisting of two gold plated nickel wires was also inserted 1.5 mm away from the grounded central electrode. A Pearson current transformer and a high voltage probe measured the electrical characteristics of the plasma. Figure 18 shows time resolved pictures with the camera looking parallel to the grounded electrode axis.

The camera was triggered by the function generator, the gate width was set at 5 ns and the gate delay was chosen to provide measurements through the rf cycle for 3 lpm, 5 lpm and 7 lpm helium flow rates. Because one rf period is $T \approx 74$ ns, 15 consecutive pictures were recorded. Donut-shaped structures were observed concentric with the grounded electrode.

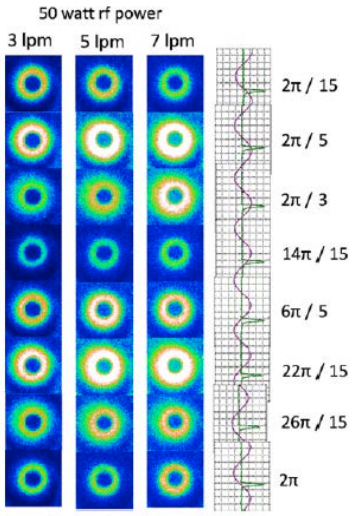

Figure 18: Phase resolved images with 5 ns gate widths over one complete rf cycle for different helium flow rates. Phases are shown on the right side of the images.

These studies found that the discharge intensities were periodic at the rf driving frequency with the brightest images at T/4 and 3T/4, where T is the rf period, taken at the discharge current peaks and also showed that the bright emitting layers got thinner and closer to the electrodes when the frequency increased.

Figure 19 gives measurements of light intensity for 50 W and 150 W of rf power and 5 lpm helium flow rate. For 50 W, one intensity peak appeared at approximately 1.5 mm. For 150 W this peak shifted to 1.9 mm and two additional peaks occurred at 4 mm and 8 mm. The intensity vs. radial position of these structures are compared in Figure 20 for powers of 50 W, 150 W and 200 W. Note that increasing the power a factor of 3 increased the emission line intensities by approximately a factor of 10 and that the plasma radius is at least 12 mm. The plasma size is much larger than the parallel plate atmospheric pressure DBDs.

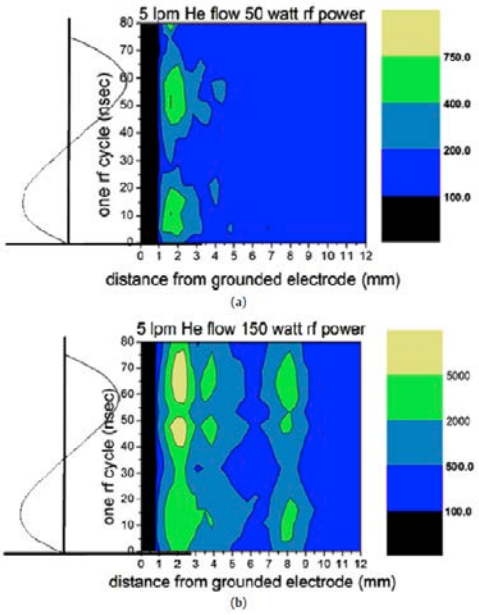

Figure 19: Time and space resolved light emission profile over one rf cycle for (a) 50 W and (b) 150 W rf power.

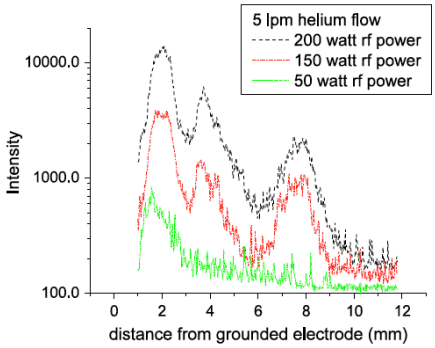

Figure 20: The radial light intensity peaks for different power.

For 50 W, the discharge peaked around the grounded center electrode and was uniform at

larger radii as shown in Figures 18 and 19a. As the power increased, the light emission intensity expanded in the radial direction. The ICCD pictures showed the presence of a double humped structure in addition to increased light emission when the input power reached 120 W. The transition in the power characteristics was identified as a mode change that resembles the α to γ mode transition observed in parallel plate atmospheric pressure discharge. In the γ mode, ionization is maintained by secondary electrons emitted from electrodes and energized by sheath electric fields. This causes localized ionization near the sheaths of both electrodes. In the α mode, bulk plasma electrons provide ionization resulting in low current densities. In the α mode, plasma stability control is easy because of gradual voltage dependence of the electron density. In addition, the increased electron temperature near the electrode sheaths increases light emission.

References: Publications and conference presentations supported by the AFOSR grant

[1] A. R. Hoskinson and N. Hershkowitz, "Modelling of dielectric barrier discharge plasma actuators with thick electrodes", J. Phys. D: Appl. Phys. 44 (2011) 085202

[2] S. Nourgostar and N. Hershkowitz, "Phase Contrast Imaging of Induced Airflow Topologies Produced by Dielectric Barrier Plasma Actuators", GEC- Salt Lake City, UT 11/18/2011

[3] S. Nourgostar and N. Hershkowitz, "Time-Resolved Phase Contrast Imaging of Induced Gas flow by a Dielectric Barrier Discharge Plasma Actuator", AVS – Nashville, TN 11/2/2011

[4] A. Gulec, L. Oksuz, and N. Hershkowitz, "Optical studies of dielectric barrier plasma aerodynamic actuators", Plasma Sources Sci. Technol. 20 (2011) 045019

[5] M. U. Siddiqui, R. Bonazza, and N. Hershkowitz, "An investigation of micron diameter exposed-electrode single barrier dielectric barrier discharges", ICOPS - Chicago, IL 6/30/2011

[6] M. U. Siddiqui, R. Bonazza, and N. Hershkowitz, "The relationship between dielectric barrier discharge performance in ambient and flowing air", GEC - Salt Lake City, UT 11/18/2011

[7] A. Gulec, L. Oksuz, and N. Hershkowitz, "Coaxial rf atmospheric pressure dielectric barrier air–helium plasma characteristics", Physics Letters A 375 (2011) 1733–1736